



Structural modeling of ZnFe_2O_4 systems using Buckingham potentials with static molecular dynamics

Óscar A. Restrepo^{a,b,*}, Óscar Arnache^a, Johans Restrepo^b, Charlotte S. Becquart^c, Normand Mousseau^d

^a Grupo de Estado Sólido-GES, Instituto de Física, Universidad de Antioquia, A.A. 1226, Medellín, Colombia

^b Grupo de Magnetismo y Simulación G+, Universidad de Antioquia, A.A. 1226, Medellín, Colombia

^c Univ. Lille, CNRS, INRA, ENSCL, Centrale Lille Institut, UMR 8207, UMET, Unité Matériaux et Transformations, F 59 000, Lille, France

^d Département de Physique and Regroupement Québécois sur les Matériaux de Pointe, Université de Montréal, Case Postale 6128, Succursale Centre-ville, Montréal, QC, H3C 3J7, Canada

ARTICLE INFO

Communicated by F. Peeters

ABSTRACT

Using Buckingham potentials we study zinc spinel ferrites ZnFe_2O_4 mechanical properties such as elastic constants, bulk moduli and vacancy formation energies E_V at zero temperature. These properties are analyzed as a function of the lattice parameter, the pressure and the inversion degree parameter. The potentials predict the geometry of normal and partial inverse spinels in good agreement with reported experimental data. Statistical randomness of the octahedral sites in partial inverse spinels is implemented to investigate its effects in energies, the lattice parameter, the elastic constants and bulk moduli. The results show that deformations of up to $\pm 6\%$ are associated with pressures of up to 50 GPa, and that the normal spinel at zero pressure is in the limit between brittle and ductile, ($B/G = 1.77$). Besides, positive pressures make the normal spinel brittle while negative ones transform it into ductile. However, the partial inverse spinels are ductile materials whose ductility increases with the inversion degree. It is also found that $E_V(\text{O}) \leq E_V(\text{Zn}) \leq E_V(\text{Fe})$ and that these computations require a large box size. Our results show that fluctuations due to randomness of Zn and Fe play an important role in the formation of vacancies in the inverse spinel and their stability, but they can be safely ignored for elastic constants. The results are compared to experimental data found in the literature.

1. Introduction

Zinc-ferrites ZnFe_2O_4 (ZFO) are an important kind of spinel structures used in advanced technological applications, such as spintronic devices, power inductors, electromagnetic interference filters, film transformers in integrated circuits, antennas, nanowires, soft magnets, li-ion batteries, etc. [1–7].

The ZFO is a zinc-ferrite having a spinel structure and -it is usually found forming a normal spinel structure, although, inverse spinel structures can also be synthesized. The ZFO crystallizes following the general stoichiometric formula $(\text{Zn}_{1-x}^{2+}\text{Fe}_x^{3+})[\text{Zn}_x^{2+}\text{Fe}_{2-x}^{3+}]\text{O}_4^{2-}$ and space group $\text{Fd } \bar{3} m$, no. 227, where () and [] stands for tetrahedral and octahedral sites respectively [8,9]. The unit cell consists of 32 O^{2-} anions organized in a face centered cubic (fcc) structure, forming 8 tetrahedral and 16 octahedral sites. From the experimental viewpoint, the most chemically stable structure of ZFO is the normal spinel structure

ZnFe_2O_4 , which has $x = 0$. When $0 < x < 1$ it is called partial-inverse ZFO spinel, which is also observed experimentally [6,10,11]. The x parameter thus plays a relevant role for structural and mechanical properties. It also has a role in other properties not studied here, e.g., a strong ferromagnetism results from partially inverse spinel structures [6, 12]. According to Granole et al. [10], the partial inverse ZFO exhibits a variable structure where the distribution of Zn and Fe cations between octahedral and tetrahedral sites within the crystal lattice depends on the synthesis conditions. Rietveld refinement and Mössbauer spectroscopy experiments show that the inversion degree increases linearly with the calcination temperature [11]. Normal ZFO can be synthesized by mixing $\alpha\text{-Fe}_2\text{O}_3$ and ZnO oxides by conventional solid state methods (milling and heating) whereas partial inverse ZFO can be prepared by other techniques such as e.g., the reaction of $\text{Zn}(\text{SO}_4)_2$ with $\text{Fe}_2(\text{SO}_4)_3$ in LiCl molten salt [6].

Although ZFO systems have been largely studied experimentally and

* Corresponding author. Grupo de Estado Sólido-GES, Instituto de Física, Universidad de Antioquia, A.A. 1226, Medellín, Colombia.
E-mail address: oantonio.restrepo@udea.edu.co (Ó.A. Restrepo).

Table 1
Buckingham spinel parameters for ZnFe₂O₄ spinel systems [25–28].

Pair	z_i	z_j	A_{ij} (eV)	ρ_{ij} (Å)	C_{ij} (eVÅ ⁶)
Zn ²⁺ O ²⁻	+2	-2	529.70	0.3581	0
Fe ³⁺ O ²⁻	+3	-2	1414.6	0.3128	0
O ²⁻ -O ²⁻	-2	-2	9547.96	0.2192	32
FeFe, ZnZn, ZnFe	(only Coulomb term used)				

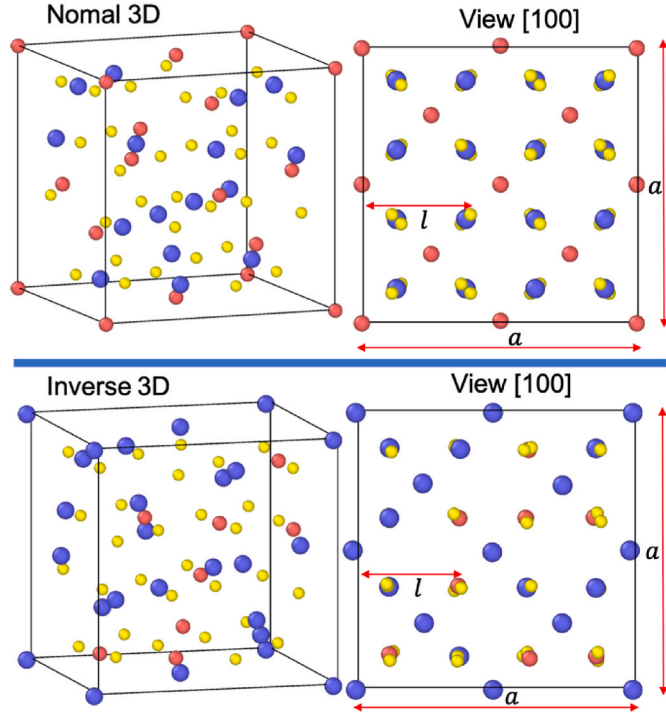


Fig. 1. 3D and top views along [100] direction of a normal ($x = 0$) and inverse ($x = 1$) ZFO spinel structures after relaxation to zero pressure with the Buckingham potential. Red is Zn, blue is Fe and yellow is O. a is the lattice, $u = l/a$ is the anion parameter and l is de distance to first O ion with coordinates $(u, u, u)a$. (For interpretation of the references to colour in this figure legend, the reader is referred to the Web version of this article.)

computationally, only a few molecular dynamics (MD) studies were performed, due, in part, to the lack of good empirical potentials or to the computational cost of the methods based on density functional theory (DFT). Indeed, most of the recent computational works are DFT studies of optical and magnetic properties, although in some cases structural properties are also analyzed [13–17]. The only classical MD simulations

Table 2

Lattice constant a (Å); final energy/atom E_f (eV); the bulk modulus B (GPa), polycrystalline data: rigidity modulus (or shear modulus) G (GPa), Young modulus E (GPa) and Poisson ratio ν_H ; the elastic constants (GPa) and the Zener anisotropic factor A . Standard deviations over 400 samples are given for inverse ($x = 1$) and partial inverse spinels ($x = 0.5$).

ZFO-Spinel	a	E_f	B	G	E	ν_H	C_{11}	C_{12}	C_{44}	A
Normal ($x = 0.0$)	8.479	-27.438	212.78	119.39	301.74	0.26	338.00	150.17	140.19	1.49
Inverse ($x = 0.5$)	8.445	-27.362	213.0	116.38	295.33	0.27	325.25	156.50	144.49	1.72
	± 0.013	± 0.004	± 3.5	± 1.00	± 2.63	± 0.00	± 6.38	± 4.50	± 3.00	± 0.10
Inverse ($x = 1.0$)	8.391	-27.327	230.49	112.16	289.52	0.29	331.73	179.88	153.03	2.02
	± 0.008	± 0.003	± 0.62	± 0.49	± 1.18	± 0.00	± 2.27	± 0.45	± 0.66	± 0.03
Normal spinel										
DFT ^(Meng [20])	8.52	-	170.30	59.10	158.91	0.34	219.20	145.84	81.36	2.22
MD ^(Lewis [18])	-	-	203.3	114.2	288.6	0.31	322	144	131	1.47
Exp ^(Lewis [18])	-	-	193.0	115.8	289.5	0.37	265	157	157	2.91
Exp ^(Grimes [42])	-	-	193.0	93.5	241.5	0.29	265	157	135	2.50
Exp ^(Li [41])	8.441	-	182.4	74.6	196.9	0.32	250.5	148.4	96.2	1.89
Exp ^(Gholizadeh [43])	8.5	-	77.7	49.91	123.3	0.23	144.3	44.42	48.9	0.98

we found are from Lewis & Catlow [18]. Also we have done a resent MD study but in Ni-Fe-O spinel strutures which share some similitities to ZFO systems [19]. Apparent discrepancies among experiments and also with some simulations, show that more simulations are needed. For example, DFT computations done on ZFO [20], at pressures of 0 GPa, 11 GPa and 23 GPa predict that the minimum value for elastic constants is at 11 GPa. This appears to contradict experiments on magnetite, that show a uniform increase with pressure for pressure ranging from 0 to 9.0 GPa [21,22]. Hence the need to explore further the impact of pressure on ZFO properties.

Another interesting parameter in these spinels is the vacancy formation energy. This is important for several reasons: first, ZFO is a well-known anode material in lithium ion batteries due to its large theoretical capacity and it is well known that point defects have an important role for lithiation [7]. Second, physicochemical properties such as photocatalysis and electrocatalysis are strongly affected by the distribution of the cations within the oxygen lattice [10,23]. For instance, hydrogenation for renewable energy processes requires ZFO flat films for photoelectrochemical performance of photoanodes for water oxidation, where O vacancies with n-type character are important [24]. Furthermore, DFT calculations suggest that oxygen vacancies can play an important role in the formation of local ferromagnetic coupling between Fe ions at octahedral sites in ZFO [17]. Besides, DFT calculations of the band structure and density of states predict that vacancies change the normal spinel ZFO from a semiconducting to a metallic character [13].

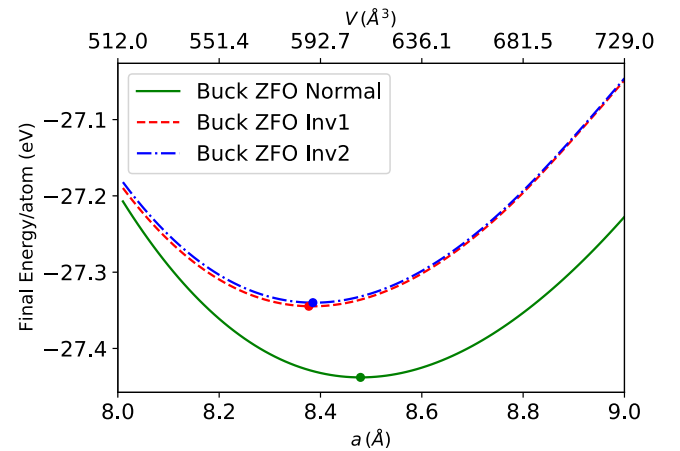


Fig. 2. ZFO structure minimization as a function of lattice a (or volume V , top axis) with the Buckingham potential. Dots are the lowest minima or zero-pressure point. Inv1 and inv2 are two random inverse spinel samples.

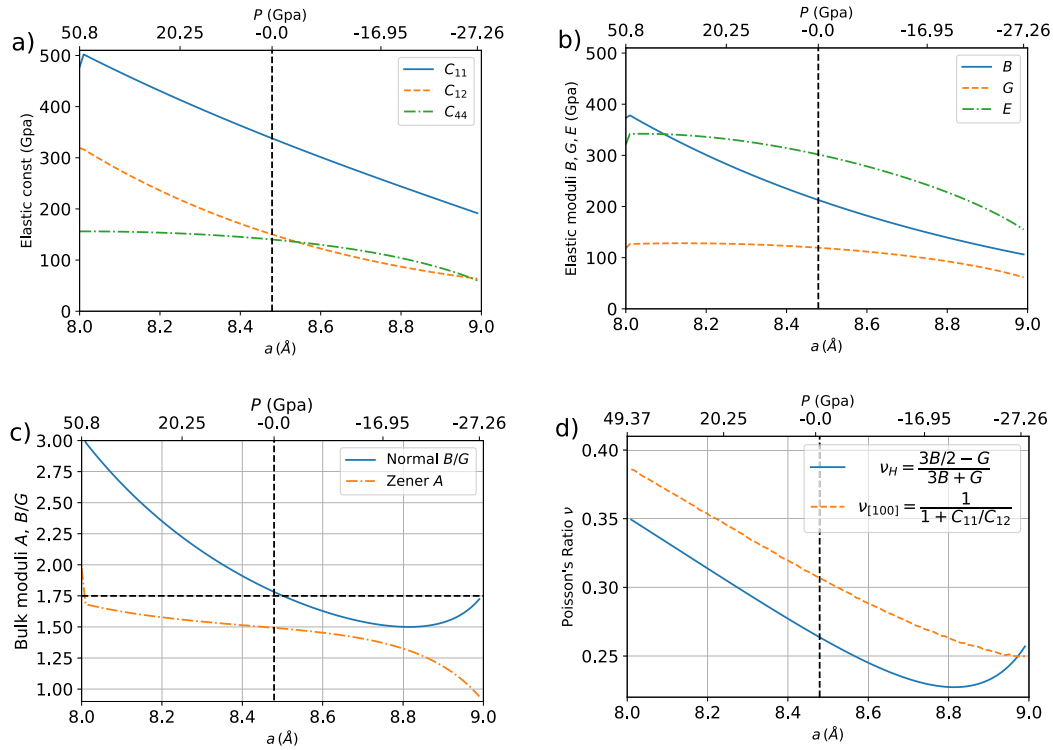


Fig. 3. In a), normal spinel elastic constants vs the lattice a and in b), the elastic moduli. The vertical dashed-line indicates zero pressure. In c), the Zener anisotropic factor A , the Pugh ratio $B/G > 1.75$, indicates that the ZFO behaves as ductile, whereas $B/G < 1.75$, the material behaves as brittle. In d), the Poisson's Ratios for a polycrystalline aggregate ν_H , and for a monocrystalline $\nu_{[100]}$ along direction [100]. Pressure P is given in top axis.

In this study, we test a combination of Buckingham pair potentials [25]. These potentials have been tested individually for systems such as zinc oxide nanobelts of ZnO [26,27] and magnetite [28]. First, we revisit the behavior of elastic properties at zero pressure for these systems and compare discrepancies found with the literature. After, we study them as a function of the lattice and pressure. We then investigate the role of the inversion degree to conclude our study with the vacancy formation energies. This paper aims to establish whether these potentials can reproduce the structural ZFO properties. In particular, we tackle the interplay between geometry and the structural behavior of ZFO spinel ferrites for structures exhibiting normal and partial-inverse configurations.

2. Methodology

2.1. Force-field

To fully characterize the ZFO spinel structure, it is necessary to model both the cation interactions — Fe–Fe, Zn–Zn and Zn–Fe— and the interactions with the O atoms — Zn–O, Fe–O and O–O. For the Zn–O, Fe–O and O–O pair interactions we employ an empirical Buckingham potential

$$V(r_{ij}) = \frac{z_i z_j e^2}{4\pi\epsilon_0 r_{ij}} + A_{ij} \exp\left(\frac{-r_{ij}}{\rho_{ij}}\right) - \frac{C_{ij}}{r_{ij}^6}, \quad (1)$$

where A_{ij} , ρ_{ij} and C_{ij} are the fitting parameters, and z_i is the charge of ion i . The cation interactions, Fe–Fe, Zn–Zn and Zn–Fe, are handled, as usual, using only a coulomb term. This is a long-range interaction potential that can be computed via particle-particle particle-mesh (PPPM) or the Ewald methods [29], here we use Ewald. The Wolf method [30, 31] can also be used in principle, however, it exhibits the poorest performance with minimizations for our system. The ZnO pair potential [27] has been tested with MD for example to reproduce the response of

zinc oxide nanobelts under tensile loading [26,27], while the FeO potential has been used to simulate some magnetite properties like diffusion [28]. The parameters are given in Table 1. Our simulations are performed using the Large-scale Atomic/Molecular Massively Parallel Simulator (LAMMPS) [32].

In the Ewald (or PPPM) method three parameters must be set: (i) the cut-off a distance r_c for computing long-range interactions into the k -space, (ii) the desired relative error ϵ in forces and, (iii) the damping parameter α . In contrast to simulations at finite temperature, the coulombic part can be cumbersome to minimize to get zero pressure as simulations may stop before reaching the predefined force tolerance. This affects the stresses and, as a consequence, the elastic constants may not be reliable. The minimization procedure may stop because the algorithm is unable to reduce the energy (from one step to the next one, the code stops if the change in energy is lower than the machine precision although the force is not yet zero, leading to wrong values of the elastic constants). A solution is to choose the r_c , ϵ and α parameters so that the Ewald sums converge rapidly. The cut-off distance is set to $r_c = 16 \text{ \AA}$ (lower values exhibit problems of convergence or do not recover the spinel structure). The precision is set to $\epsilon = 10^{-10}$ (this value is small compared to usual values reported to be around $\sim 10^{-4}$ [28] for MD simulations at finite temperatures, however, the precise computation of static elastic constants requires higher precision). The damping parameter chosen is the predefined value computed by LAMMPS code at the defined precision which guarantees a full relaxation for the smallest system (the unitary cell), then this value is kept for the larger similar system. Adding the long-range term r^{-6} does not modify the results, so only r^{-1} is computed in the k -space. For computing vacancy properties, the energy must be corrected by adding a background $E_{bg} = -\frac{\pi}{2\epsilon^2 V} \left(\sum_{i=1}^N z_i\right)^2$ to satisfy charge neutrality in the Ewald sum [33]. This is easily handled by LAMMPS.

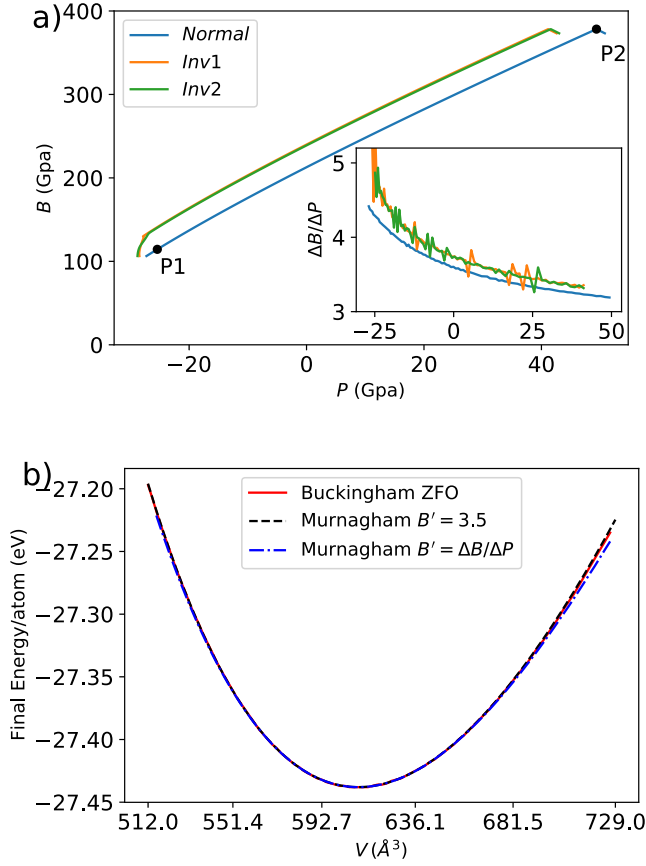


Fig. 4. a) Bulk modulus B and its derivative as a function of pressure P and b) the corresponding Energy as given by Buckingham potential and the Murnaghan's equation for a normal spinel, using $B' \approx 3.5$ (slope between P1 and P2) or $B'(P) \approx \Delta B/\Delta P$ in a normal spinel (inverse case not shown).

2.2. Elastic constants

The computational procedure to obtain the elastic constants relies on minimizations and they are done using the conjugate gradient (CG) algorithm set by default in LAMMPS. The procedure starts by computing the six stress components over all N particles in the system [34,35], namely

$$P_{ij} = \frac{1}{V} \sum_{k=1}^N (m_k v_{ki} v_{kj} + r_{ki} f_{kj}), \quad (2)$$

where r_{ki} , v_{ki} and f_{ki} are the vector components of the k^{th} -atom in the i direction of the position, velocity and force respectively. In minimizations, the first sum is not considered. This gives a symmetric stress tensor, stored as a 6-element vector, with the components ordered by xx , yy , zz , xy , xz , yz . The pressure is computed from the stress tensor as the average

$$P = \frac{P_{11} + P_{22} + P_{33}}{3} = \frac{1}{3V} \sum_{k=1}^N (r_{ki} f_{k1} + r_{k2} f_{k2} + r_{k3} f_{k3}). \quad (3)$$

The elastic constants are related to the stress tensor by the relation $C_{\alpha\beta} = -\frac{\partial P_\alpha}{\partial e_\beta}$, where e_β is the strain tensor and the indices run over the previous six ordered components. To do so, the simulation box is minimized to get zero pressure. Next, the box is deformed by a small positive fraction and minimized again to get the stress tensor after the deformation $C_{\alpha\beta}^+$ (a force tolerance of 10^{-5} eV/ \AA with energy tolerance set to 0.0 eV is used in all minimizations); the procedure is then repeated

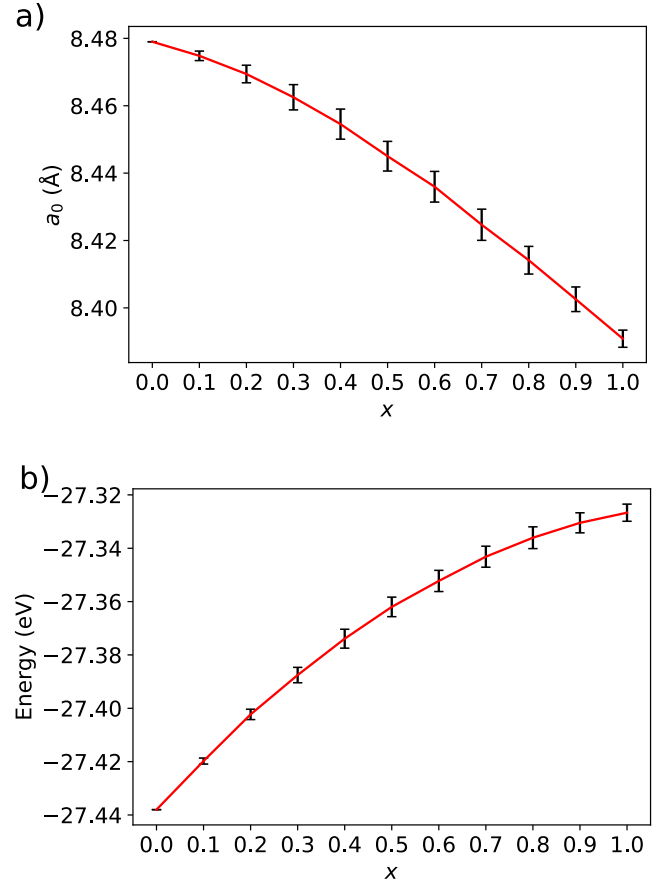


Fig. 5. In a) lattice and in b), energy vs inversion degree x . Statistical fluctuations, indicated by bars, are computed by the standard deviation.

for a negative fraction to get $C_{\alpha\beta}^-$, and elastic constants are the average $C_{\alpha\beta} = (C_{\alpha\beta}^+ + C_{\alpha\beta}^-)/2$ [19]. Once the elastic constants are obtained, we compute the physical quantities of interest for a polycrystalline aggregate, i.e. the bulk modulus B , the rigidity modulus (or shear modulus) G , the Young modulus E , the Poisson ratio ν_H , using the Voigt-Reuss-Hill scheme [36,37]:

$$B = \frac{C_{11} + 2C_{12}}{3}, \quad (4)$$

$$G = \frac{G_R + G_V}{2}, \quad (5)$$

$$G_V = \frac{(C_{11} - C_{12}) + 3C_{44}}{5}, \quad (6)$$

$$G_R = \frac{5(C_{11} - C_{12})C_{44}}{3(C_{11} - C_{12}) + 4C_{44}}, \quad (7)$$

$$E = \frac{9GB}{G + 3B}, \quad (8)$$

$$\nu_H = \frac{3B/2 - G}{G + 3B} = \frac{1}{2} \left(1 - \frac{3G}{3B + G} \right) = -1 + \frac{E}{2G} = \frac{3B - E}{6B} = \frac{1}{2} - \frac{E}{6B}. \quad (9)$$

Since the spinel is anisotropic, we also compute Poisson's ratio for a monocrystalline structure along the [100] direction according to

$$\nu_{[100]} = \frac{1}{1 + \frac{C_{11}}{C_{12}}}. \quad (10)$$

In fact, Poisson's ratio is most simply expressed as a ratio of

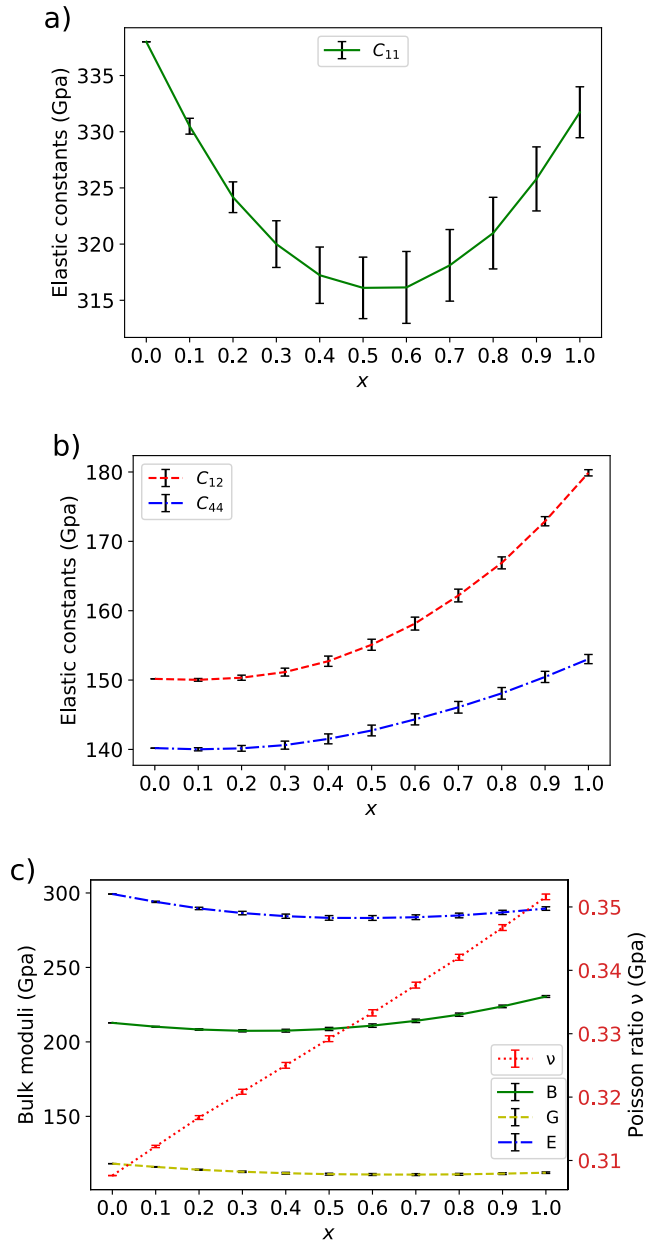


Fig. 6. Elastic constants and Bulk moduli as function of the inversion degree x .

compliance coefficients, $\nu_{ij} = -S_{ij}/S_{ii}$ (the compliance is the inverse $S = C^{-1}$), with $i \neq j$ [38,39]. Because of symmetry in cubic spinels, $\nu_{ij} = \nu_{ji}$, where $\nu_{100} = \nu_{12} = \nu_{13} = \nu_{23}$ and the others $\nu_{ij} = 0$, for $i, j = 4, 5, 6$. Elastic anisotropy can also be measured by the Zener anisotropic factor

$$A = \frac{2C_{44}}{C_{11} - C_{12}}. \quad (11)$$

Spinel structures must be mechanically stable and as a consequence, their elastic constants must satisfy the stability criteria [36],

$$C_{11} > 0, C_{44} > 0, C_{11} > |C_{12}|, (C_{11} + 2C_{12}) > 0. \quad (12)$$

2.3. Geometrical construction

Partial inverse spinels are described by the formula $(Zn_{1-x}^{2+}Fe_x^{3+})[Zn_x^{2+}Fe_{2-x}^{3+}]O_4^{2-}$, thus, they can be constructed using a simple Monte Carlo method. We randomly place Fe or Zn cations with probability equal to the inversion parameter x in the following manner:

a random number $0 \leq r \leq 1$ is generated; for a tetrahedral site, if $r \leq x$ we put an Fe ion on the site, otherwise a Zn ion is placed. For an octahedral site, if $r \leq x/2$ we put a Zn ion, otherwise an Fe ion. However, this method does not guarantee that when $x = 1$, i.e. for the full inverse spinel, all tetrahedral sites are filled with Fe ions (the same applies for octahedral sites). In that case, we put Fe ions in the tetrahedral sites and shuffle half Fe and half Zn ions on octahedral sites using the Fisher-Yates algorithm [40].

3. Results and discussion

3.1. Geometries and elastic constants at zero pressure

In the following results a unitary cell is used with normal spinels and a box of $3 \times 3 \times 3$ unitary cells with inverse spinels to reduce fluctuations and get better statistics. Both the inverse and normal spinels are stable after energy minimizations to zero pressure (Fig. 1). The lattice constants predicted are in good agreement with experiments [41], as reported in Table 2. The anion parameter u is required to define fractional coordinates of O ions and in an ideal spinel it has the value of $3/8$ (Wyckoff notation, point symmetry $\bar{4}3m$) [8]. As expected, in a normal spinel this potential predicts a larger anion parameter (0.392), which is close to the experimental values (0.383) [15] or (0.386) [34] or the DFT value (0.384) [15].

Fig. 2 shows the minimum energy as a function of the lattice parameter (or the volume in the top axis). We perform a series of simulations as a function of the lattice parameter a where a varies between 8.0 \AA and 9.0 \AA (or equivalently, we vary the volume from 512 \AA^3 to 729 \AA^3) where the spinel structure is expected to remain stable and with steps of 0.1 \AA (this is equivalent to producing a strain of approximately $\varepsilon = \frac{|a-a_0|}{a_0} \sim 6\%$, where a_0 is the lattice parameter at zero pressure). For the inverse spinel we look at two different random samples referred to as Inv1 and Inv2. As expected, the plots of the energy with this potential (see Fig. 2) predict the normal spinel as the most stable structure.

Bulk physical properties predicted by the potential after energy minimization at zero pressure are computed and also given in Table 2. The respective results are compared both with DFT and experiments from literature [18,41,43]. The predicted elastic constants satisfy the stability conditions (equation (12)) but they are larger than experimental and DFT results. For inverse spinels, we perform 400 simulations at zero pressure, each by randomly shuffling ions over octahedral compositions. Averages and standard deviations are computed for inverse degrees of 0.5 and 1.0. The lattice constants predicted for the partial inverse spinel and the inverse spinel are smaller than that of a normal spinel by $\sim 0.5\%$ and 1.1% respectively.

As shown in Table 2, experimental data for elastic constants of a ZFO-normal spinel vary greatly. Our results are closer to the experimental results reported by Lewis and Catlow [18], with differences of $\sim 27\%$, $\sim 4\%$ and $\sim 11\%$ for C_{11} , C_{12} and C_{44} respectively. They are also similar to the MD study by the same group, performed with a Shell-model potential of their own. While our results are of similar precision for C_{11} ($\sim 32\%$) and C_{12} ($\sim 1.2\%$) with respect to Li et al. experiments [41], agreement is much less for C_{44} ($\sim 46\%$). The difference on C_{44} is even larger when compared to DFT results reported by Meng et al. [20] ($\sim 72\%$). For C_{11} the difference is large too ($\sim 30\%$) although C_{12} ($\sim 3\%$) is similar to ours. Experimentally, in spinel ferrites, it is expected that C_{44} be the smallest of the modulus [41], as observed in Table 2, except for Lewis' experiment where it seems that the Cauchy relation applies as $C_{12} = C_{44} = 157 \text{ GPa}$. However, the Cauchy relation is not expected to hold for these spinels, i.e., C_{12} should not be equal to C_{44} , because they are not centrosymmetric [44,45]. This is indeed observed by Grimes [42] where $C_{44} = 135 \text{ GPa}$ (see Table 2). We note that Gholizadeh [43] experimental results, presented here for completeness, are for nanoparticles, far from the bulk condition, which explains why they stand out.

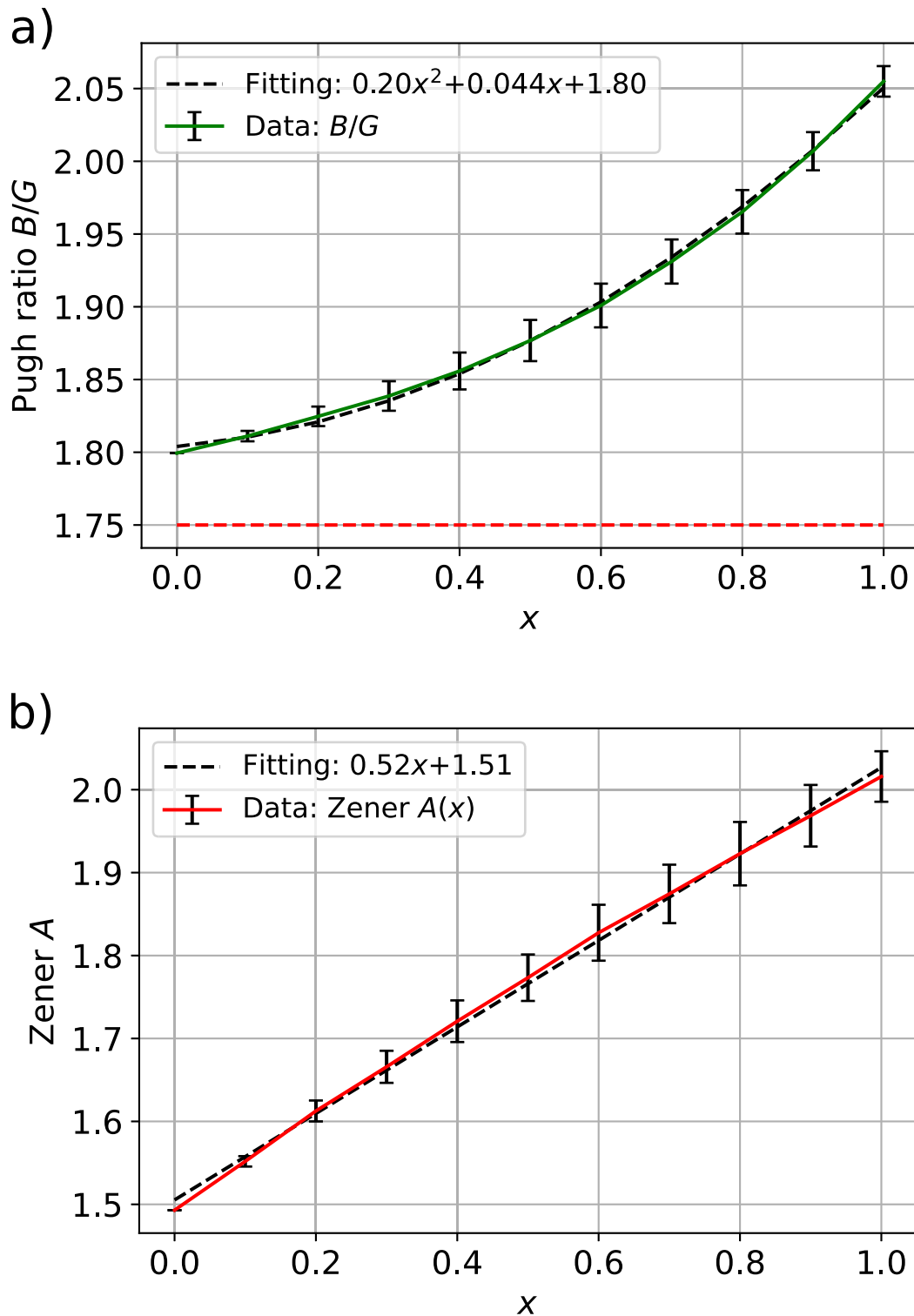


Fig. 7. a) Ductile behavior of the ZFO partial inverse spinel versus the inversion degree x ; red line, $B/G = 1.75$ is the limit between ductile and brittle. b) The Zener anisotropy factor. (For interpretation of the references to colour in this figure legend, the reader is referred to the Web version of this article.)

Results for inverse and partial inverse spinels are also summarized in Table 2. While we did not find experimental data nor DFT results to compare with, we expect a precision similar to that of normal spinels as the cation random mixing in octahedral sites does not affect the lattice parameter and the final energy significantly (Table 2). This is also observed in the error given for rigidity moduli B , G and E (less than

$\sim 1\%$) and in the case of the elastic constants (around $\sim 2\%$) for the inverse case.

3.2. Effects of lattice and pressure changings

We also compute the evolution of elastic properties and pressure as a

Table 3

Vacancy formation energies, E_V (eV), for normal and inverse (Inv: $x = 1$) ZFO spinels. For the inverse box $1 \times 1 \times 1$ the average is over 10 samples (or 560 ions), and for the others only one sample is used and averaging over the total number of ions.

Vacancy	Zn	Fe	O
Buck $1 \times 1 \times 1$	4.48	4.88	1.80
Buck $4 \times 4 \times 4$	5.79	7.68	3.03
Buck $10 \times 10 \times 10$	5.99	8.11	3.22
Buck $1 \times 1 \times 1$ (Inv)	2.19 ± 0.31	6.30 ± 1.34	1.55 ± 0.69
Buck $4 \times 4 \times 4$ (Inv)	3.52 ± 1.24	8.41 ± 2.29	2.48 ± 1.76
Buck $5 \times 5 \times 5$ (Inv)	3.57 ± 1.52	8.54 ± 2.55	2.53 ± 1.96
DFT [13,51]	1.99	5.46	7.07

function of the lattice parameter, as shown in Fig. 3a and b. The potential predicts that under compression of around $\sim 6\%$ the pressure rises up to 50 GPa but the structure remains stable. C_{11} and B varies linearly with the lattice while C_{12} increases faster under compression and C_{44} is approximately constant (although it diminishes beyond $a > 8.7 \text{ \AA}$).

As the lattice parameter is expanded and the pressure falls, effects on B , G and E become important: a compression of $\sim 6\%$ produces an increase in the bulk modulus of ~ 170 GPa while an expansion of the same amount leads to a reduction to ~ 120 GPa. Under expansion, the shear modulus G shows a slow variation while the Young modulus E falls rapidly, as the ZFO becomes less stable. Under this range of pressures, we observe that $B > G$, which indicates that the shear modulus is the parameter that limits the mechanical stability. The Pugh ratio B/G (Fig. 3c) is a useful criterion to distinguish between ductile and brittle behavior: if $B/G > 1.75$, the material behaves as ductile, whereas if $B/G < 1.75$, the material behaves as brittle [20,46]. We observe that $B/G > 1.75$ for positive pressures, which indicates that the spinel is ductile, whereas for negative pressures $B/G < 1.75$ and the spinel becomes brittle.

Because Poisson's ratio is proportional to the plasticity of materials it reflects their stability and provides information about the interatomic forces [20]. According to equation (9), in an isotropic material, Poisson's ratio is restricted to $-1 \leq \nu_H \leq 0.5$ ($B = 0$ or $G = 0$). However for two body central-forces in polycrystalline aggregates (formed, e. g, by fcc, bcc or crystallites like NaCl, ZnS, CsCl), ν_H is bounded to $0.25 \leq \nu_H \leq 0.5$ [47,48]. Since spinels are not centrosymmetric, the central-force model predicts a violation of the Cauchy's relation, i.e. that $C_{12} \neq C_{44}$ and these bounds do not apply [44,45]. In a normal spinel, at zero pressure, the potential predicts $\nu_H = 0.26$ and $\nu_{[100]} = 0.31$. As the lattice

is expanded, ν_H falls below 0.25, whereas $\nu_{[100]}$ is bounded to 0.25–0.5 limits. Fig. 3d shows that $\nu_H < \nu_{[100]}$. The difference is almost constant (~ 0.04) from 8.0 \AA to 8.8 \AA interval, but beyond 8.8 \AA ν_H has a minimum and starts to increase. This is also observed for the Zener anisotropy factor A in Fig. 3c. In general, a material is elastically isotropic if A is equal to one, otherwise it is elastically anisotropic. Our plot of A indicates that ZFO is not isotropic, in agreement with experimental results of Li or Lewis (see Table 2).

We also compare to the Murnaghan's equation, which is an empirical functional form of the third-order representation of the energy as a function of volume and pressure, and that can be used to calculate the derived structural properties [49]. It has the form

$$E(V) = E_0 - \frac{B_0 V_0}{B' - 1} + \frac{B_0 V}{B'} \left[\frac{(V_0/V)^{B'}}{B' - 1} + 1 \right], \quad (13)$$

where E_0 , V_0 , and B_0 are the total energy, volume, and bulk modulus at zero pressure of the unit cell. The derivative $B' = dB/dP$ is usually assumed to be a constant, B'_0 , in the derivation of Murnaghan's equation (13). Fig. 4 shows the plots of the bulk modulus and its derivative (inset plot) versus pressure, as predicted by the Buckingham potential for a ZFO-normal spinel. Although the evolution of the bulk modulus with pressure is almost linear, $B(P) = B_0 + B'_0 P$, i.e. it can be approximated by a straight line of slope $B'_0 = 3.5$ between points P1 and P2. Note that a better approximation is to consider $B'(P) \approx \Delta B/\Delta P$ as in the inset figure. These approximations are used to plot Murnaghan's equation, using a cubic spline interpolation, and then comparing to the energy found with the Buckingham potential. We observe that the later approximation of B' performs better.

3.3. Inversion degree: normal vs partial ZFO systems

To better understand the behavior of the ZFO Buckingham potential, we carried out a study of the mechanical properties as a function of the inversion degree x . Data were averaged over 400 simulations, each with a different random choice of cationic distribution in octahedral sites. Fig. 5a shows the x -dependence of the lattice parameter and the energy, with the bar showing the standard deviations observed over the 400 realizations. As the inversion degree increases, a reduction of the lattice parameter takes place with a consequent energy cost given in Fig. 5b, thus destabilising the partial inverse spinels when compared to the normal one. This is in agreement with experiment, where a lattice parameter of $8.441(7) \text{ \AA}$ for a normal ZFO and a smaller value of 8.377

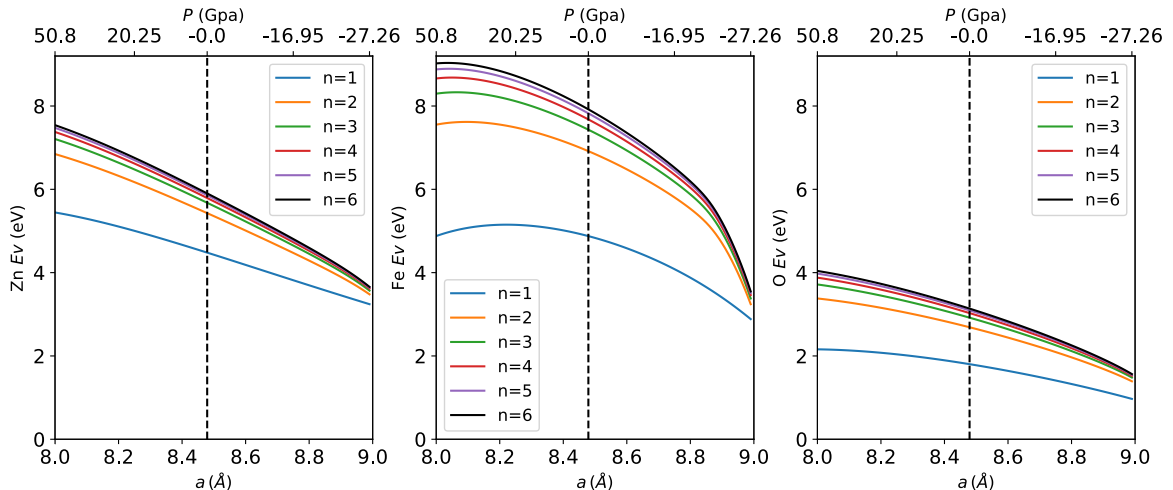


Fig. 8. Vacancy formation energies E_V as a function of the lattice parameter (bottom) and pressure (top) for six different box sizes for the ZFO normal samples. Dashed lines indicate the zero pressure limit. $n = 1$, means a vacancy per cell whereas $n = 6$ means a vacancy per 6^3 cells.

(6) Å for a partial inverse with $x = 0.59$ were reported [6]. The standard deviation associated with the disorder is maximal at around $x = 0.6$. These reduce with larger box sizes and resulting self-averaging.

A similar study was done for the elastic constants and the rigidity moduli. The results are shown in Fig. 6. These vary relatively in the interval: the maximum variation for C_{12} is $\sim 20\%$ whereas for C_{11} it is $\sim 6\%$. However, a more detailed view as shown in Fig. 6, tells us that C_{11} exhibits a parabolic behavior, being symmetric with respect to $x = 0.5$, whereas C_{12} and C_{44} increase with x . A similar behavior is observed for the bulk moduli.

For the partial inverse spinels, the potential predicts a ductile behavior as shown by the analysis of the Pugh ratio where $B/G > 1.75$ [20]; see Fig. 7. In fact, the averages follow a quadratic fitting, $B/G = 0.2x^2 + 0.04x + 1.8$. The Zener anisotropy factor behaves almost linearly in the interval, following the equation, $A(x) = 0.52x + 1.51$.

We conclude that elastic constants, bulk moduli and lattice parameter are relatively sensitive to the degree of inversion (e.g. in Fig. 6b we observe that C_{44} has the largest variation of $\sim 16\%$ when changing from normal to inverse structure). However, these properties are relatively insensitive to fluctuations, which in all cases are smaller than $\sim 6\%$.

3.4. Vacancy formation energies

The vacancy formation energy E_V is the energy needed to create a vacancy defect in a perfect crystal, i.e., how much cohesive energy is needed to form a vacancy defect. For a monatomic system it can be computed using the well-known formula

$$E_V = E'_t - \frac{N-1}{N}E_t, \quad (14)$$

where E'_t is the energy computed after removing an atom and relaxation of the crystal and E_t is the total energy of a perfect crystal with N atoms also obtained after relaxation of the system. However, in spinel systems, like in concentrated alloys, different ion types contribute with different fractions to the energy. Therefore, we correct the previous formula by considering the fraction contribution of each ion type

$$E_V = E'_t - \frac{N_1-1}{N_1}E_{t1} - E_{t2} - E_{t3} = (E'_t - E_t) + \frac{E_{t1}}{N_1}, \quad (15)$$

where E_{ti} are total energies by ion type i in the perfect crystal and N_1 is the number of ions of type 1 where the vacancy is created, with $E_t = E_{t1} + E_{t2} + E_{t3}$ and $N = N_1 + N_2 + N_3$. The predicted E_V for the ZFO spinel are summarized in Table 3 and compared to DFT predictions [13]. In that DFT work, E_V is computed using the formula

$$E_V = (E'_t - E_t) + E_X, \quad (16)$$

where E_X is the reference energy of one ion X obtained from its pure crystal, bcc for Fe, hcp for Zn and for O, half the energy of the O_2 molecule: $\frac{1}{2}E(O_2)$ [50]. E_X can also be interpreted as the chemical potential of ion X [51]. E_X cannot be computed with (16) because for cation-cation interactions we only have repulsive terms. However, comparing to (15) we see that $E_X \approx E_{t1}/N_1$ taking into account the spinel structure.

The first observation is that E_V is not well predicted by using a box of $1 \times 1 \times 1$ and it is even questionable for a size of $4 \times 4 \times 4$. The DFT results are thus also questionable because of the size cell used ($2 \times 2 \times 2$ [13]). Interestingly, $E_V(\text{Fe})$ is the most affected by the size. Indeed, our results show that a larger cell of $10 \times 10 \times 10$ is required to warrant a good convergence for this property. Also, it is observed that Buckingham predicts $E_V(\text{O}) \leq E_V(\text{Zn}) \leq E_V(\text{Fe})$, whereas DFT predicts $E_V(\text{Zn}) \leq E_V(\text{Fe}) \leq E_V(\text{O})$, i.e., the Zn and Fe vacancies are more stable and the O vacancy is the easiest to create which is in contrast to DFT results.

In the case of the inverse spinel, due to its random nature, E_V should have to be computed for each ion and for different samples with the

same inversion degree, so a distribution should be expected. Due to the computational cost, we have only tried with an inverse system ($x = 1$) and up to a size of $5 \times 5 \times 5$ (minimizations over 7000 vacancies), which is acceptable. Stresses produced by the randomization manifest as fluctuations of E_V up to 35% (Zn), 27% (Fe) and 71% (O) with respect to their means. Increasing the box size does not reduce the fluctuations, but the means tend to increase as in the normal spinel case. It is also observed that E_V values for a normal spinel fall within the interval of error of the respective inverse cases. The same kind of fluctuations should be expected in DFT but their computational cost makes them too difficult to obtain.

Fig. 8 clearly shows the size effects on E_V when it is plotted as a function of lattice and pressure for six different system sizes. The results can be interpreted in terms of the vacancy densities: when $n = 1$, it means a vacancy per cell while $n = 6$, means a vacancy per 6^3 cells so there are less vacancy-vacancy interactions; as n increases E_V converges to a fixed value. As compared to Table 3, E_V (Fe) is the most affected.

Finally, it seems that most, if not all, of the calculations presented here could have been carried out with DFT, perhaps by using fewer than 400 cells to average out properties for the disordered systems. This would have provided much more robust predictions. The answer to this is not so simple. DFT could indeed have been used to get elastic properties using a small supercell. However most of the computations done here—especially for inverse structures—require large box sizes and computations of averages make the calculations impossible for DFT. Some of the calculations presented here for the inversion degree, required a cluster running for several days. In particular, in the case of the vacancy formation energy, the results require large box sizes (supercells) up to $10 \times 10 \times 10$ impossible for DFT (and almost impossible for MD for the case of inverse spinel: we were only able to compute this particular energy in $5 \times 5 \times 5$ unit cells due to the number of minimizations). Thus the need for empirical potentials and one of our goal was thus to check the Buckingham potentials.

4. Conclusions

We have used Buckingham potentials found in the literature to investigate the mechanical properties of ZFO spinels. The potentials predict the geometry of normal and partial inverse spinels in good agreement with the reported experimental data for the lattice and anion parameters. The simulations indeed predict the normal spinel as the most stable structure.

For partial inverse spinel samples, a statistical randomization of the octahedral sites is achieved to investigate its effects over energies, the lattice parameter, the elastic constants and bulk moduli. In most cases fluctuations are smaller than 6%, indicating that the randomness of the cation location in octahedral sites (Zn, Fe) is not an important factor for the elastic constants and the bulk moduli. However, randomness has an important role for vacancy formation energy E_V as large fluctuations of up to 71% (O case) are observed and in contrast to the other fluctuations, these do not seem to reduce with the system size.

In contrast to DFT that predicts $E_V(\text{Zn}) \leq E_V(\text{Fe}) \leq E_V(\text{O})$, we have found that Buckingham potentials predict $E_V(\text{O}) \leq E_V(\text{Zn}) \leq E_V(\text{Fe})$, so O ions have the lowest E_V . Also, care should be taken when interpreting DFT predictions of E_V because a cell of size $2 \times 2 \times 2$ is not large enough. In fact, we need a large box of $10 \times 10 \times 10$ to have converged results. However, this large box size does not explain the discrepancies of our results with DFT. These differences could be due to the fixed partial charges as implemented here that prevent the full applicability of the Buckingham potentials to point defects as such vacancies, a problem already known for the latent heat release during adatom condensation [52]. Such types of problems could be treated by more sophisticated approaches such as Streitz and Mintmire potential [53,54], that allows self-consistent evaluation of charge distributions. However, no parameterizations are known yet for this ternary system.

The potential predicts that deformations of up to $\pm 6\%$ can produce

pressures of up to 50 GPa, and that the normal spinel at zero pressure is in the limit between brittle and ductile, ($B/G = 1.77$) but the partial inverse spinels are ductile materials. However positive pressures make the normal spinel to be brittle while negative values transform it in ductile.

Another important aspect regarding the impacts of the synthesis on the physical properties of ferrites, is related to ZFO thin films. Substrate effects exert forces or strains on the ZFO crystalline structure and produce changes in its structural parameters. We have manufactured ZFO thin films by sputtering system, where the ZFO film was grown under Ar/O₂ mixture with a ratio of 1:2, which results in a lattice mismatch between the film and the substrate of around 3.9%, causing an enhancing of the saturation magnetization for the ZFO in thin films unlike the samples in bulk [55]. Hence, surface studies will be done in the near future.

In spite of some limitations, the combination of Buckingham potentials presented here is therefore a useful tool for further studying the mechanical and structural properties of the important ZFO spinels under conditions that are unreachable by current available modeling approaches.

Credit author statement

Óscar A. Restrepo: Investigation, Conceptualization, Methodology, Software, Data curation, Writing – original draft, Visualization. **Óscar Arnache:** Validation, Writing – review & editing. **J. Restrepo:** Validation, Writing – review & editing. **Charlotte S. Becquart:** Validation, Writing – review & editing. **Normand Mousseau:** Validation, Writing – review & editing, Cluster resources.

Declaration of competing interest

The authors declare that they have no known competing financial interests or personal relationships that could have appeared to influence the work reported in this paper.

Data availability

No data was used for the research described in the article.

Acknowledgements

This work was supported in part by grants from the Natural Sciences and Engineering Research Council of Canada (NSERC). We are grateful to Calcul Québec/Compute Canada (CQ/CC) for generous allocations of computer resources. O. R. and J. R. acknowledges University of Antioquia for the exclusive dedication program and to the CODI-UdeA 2020–34211 and CODI-UdeA 2017–16253 projects for financial support.

References

- [1] Z.Ž. Lazarević, Č. Jovalekić, A. Milutinović, D. Sekulić, V.N. Ivanovski, A. Rečnik, B. Cekić, N.Ž. Romčević, *J. Appl. Phys.* 113 (2013), 187221.
- [2] K. Shimokawa, T. Atsumi, M. Harada, R.E. Ward, M. Nakayama, Y. Kumagai, F. Oba, N.L. Okamoto, K. Kanamura, T. Ichitsubo, *J. Mater. Chem.* 7 (2019), 12225.
- [3] M. Goodarz Naseri, E.B. Saion, A. Kamali, *ISRN Nanotechnology* 2012 (2012) 1.
- [4] M. Virumbrales, R. Sáez-Puche, V. Blanco-Gutiérrez, M.J. Torralvo-Fernández, *J. Phys. Chem. C* 121 (2017) 4029.
- [5] Y.-C. Liang, H.-Y. Hsia, *Nanoscale Res. Lett.* 8 (2013) 537.
- [6] J. Wu, N. Li, J. Xu, Y. Jiang, Z.-G. Ye, Z. Xie, L. Zheng, *Appl. Phys. Lett.* 99 (2011), 202505.
- [7] H. Guo, A.C. Marschilok, K.J. Takeuchi, E.S. Takeuchi, P. Liu, *ACS Appl. Mater. Interfaces* 10 (2018).
- [8] K.E. Sickafus, J.M. Wills, N.W. Grimes, *J. Am. Ceram. Soc.* 82 (2004) 3279.
- [9] C. Yao, Q. Zeng, G.F. Goya, T. Torres, J. Liu, H. Wu, M. Ge, Y. Zeng, Y. Wang, J. Z. Jiang, *J. Phys. Chem. C* 111 (2007), 12274.
- [10] L.I. Granone, K. Nikitin, A. Emeline, R. Dillert, D.W. Bahnemann, *Catalysts* 9 (2019) 434.
- [11] L.I. Granone, A.C. Ulpe, L. Robben, S. Klimke, M. Jahns, F. Renz, T.M. Gesing, T. Bredow, R. Dillert, D.W. Bahnemann, *Phys. Chem. Chem. Phys.* 20 (2018), 28267.
- [12] J.D. Arboleda, O. Arnache, M.H. Aguirre, R. Ramos, A. Anadón, M.R. Ibarra, *Solid State Commun.* 270 (2018) 140.
- [13] J. Yao, Y. Li, X. Li, X. Zhu, *Metall. Mater. Trans.* 47 (2016) 3753.
- [14] X.F. Zhu, L.F. Chen, *J. Magn. Magn. Mater.* 323 (2011) 3138.
- [15] S. Soliman, A. Elfalaky, G.H. Fecher, C. Felser, *Phys. Rev. B* 83 (2011), 085205.
- [16] C.J. O'Brien, Z. Rák, D.W. Brenner, *J. Phys. Condens. Matter* 25 (2013), 445008.
- [17] C.E. Rodríguez Torres, F. Golmar, M. Ziese, P. Esquinazi, S.P. Heluani, *Phys. Rev. B* 84 (2011), 064404.
- [18] G.V. Lewis, C.R.A. Catlow, *J. Phys. C Solid State Phys.* 18 (1985) 1149.
- [19] Óscar Restrepo, Óscar Arnache, J. Restrepo, Charlotte S. Becquart, Normand Mousseau, *Comput. Mater. Sci.* 213 (2022) 111653.
- [20] Y. Meng, et al., *Mater. Sci. Eng.* 569 (2019), 022016.
- [21] H.J. Reichmann, S.D. Jacobsen, *Am. Mineral.* 89 (2004) 1061.
- [22] D. Errandonea, in: F.J. Manjon, I. Tiginyanu, V. Ursaki (Eds.), *Pressure-Induced Phase Transitions in AB₂X₄ Chalcogenide Compounds*, Springer Berlin Heidelberg, Berlin, Heidelberg, 2014, pp. 53–73.
- [23] Y. Hinuma, S. Mine, T. Toyao, T. Kamachi, K. Shimizu, *Phys. Chem. Chem. Phys.* 23 (2021), 23768.
- [24] A. Polo, C.R. Lhermitte, M.V. Dozzi, E. Selli, K. Sivula, *Surfaces* 3 (2020) 93.
- [25] R.W. Grimes, G. Busker, M.A. McCoy, A. Chronos, J.A. Kilner, S.-P. Chen, *Ber. Bunsen Ges. Phys. Chem.* 101 (1997) 1204.
- [26] D.J. Binks, *Computational Modeling of Zinc Oxide and Related Oxide Ceramics*, Department of Chemistry, University of Surrey, Harwell, England, 1994.
- [27] A.J. Kulkarni, M. Zhou, F.J. Ke, *Nanotechnology* 16 (2005) 2749.
- [28] J. Vaari, *Solid State Ionics* 270 (2015) 10.
- [29] C.J. Fennell, J.D. Gezelter, *J. Chem. Phys.* 124 (2006), 234104.
- [30] D. Wolf, P. Keblinski, S.R. Phillpot, J. Eggebrecht, *J. Chem. Phys.* 110 (1999) 8254.
- [31] E.E. Gdoutos, R. Agrawal, H.D. Espinosa, *Int. J. Numer. Methods Eng.* 84 (2010) 1541.
- [32] S. Plimpton, *J. Comput. Phys.* 117 (1995) 1.
- [33] V. Ballenegger, A. Arnold, J.J. Cerdà, *J. Chem. Phys.* 131 (2009), 094107.
- [34] S.L. Teich-McGoldrick, J.A. Greathouse, R.T. Cygan, *J. Phys. Chem. C* 116 (2012), 15099.
- [35] A.P. Thompson, S.J. Plimpton, W. Mattson, *J. Chem. Phys.* 131 (2009), 154107.
- [36] M. Jamal, S. Jalali Asadabadi, I. Ahmad, H.A. Rahnamaye Aliabad, *Comput. Mater. Sci.* 95 (2014) 592.
- [37] R. Hill, *Proc. Phys. Soc.* 65 (1952) 349.
- [38] A.D. Zoe, R.I. Walton, A.S.H. Marmier, C.W. Smith, K.E. Evans, *Acta Mater.* 58 (2010) 6444.
- [39] T.T.C. Ting, *Anisotropic Elasticity: Theory and Applications*, 1996, Oxford University Press, New York, 2020, <https://doi.org/10.1093/oso/9780195074475.001.0001>. Oxford Scholarship Online.
- [40] R.A. Fisher, F. Yates, *Statistical Tables for Biological, Agricultural and Medical Research*, Oliver and Boyd, London, 1948, pp. 26–27.
- [41] Z. Li, E. Fisher, J. Liu, M.V. Nevitt, *J. Mater. Sci.* 26 (1991) 2621–2624.
- [42] N.W. Grimes, *Phys. Status Solidi* 58 (1973) K129.
- [43] Gholizadeh Ahmad, *J. Nanoanalysis.* 5 (2018) 7–16.
- [44] C. Sammis, *Geophys. J. Int.* 29 (1972) 15.
- [45] M.E. Striefler, G.R. Barsch, *J. Phys. Chem. Solid.* 33 (1972) 2229.
- [46] S.F. Pugh, The london, Edinburgh, and Dublin, *Philosophical Mag. J. Sci.* 45 (1954) 823.
- [47] O.L. Anderson, H.H. Demarest Jr., *J. Geophys. Res.* 76 (1971) 1349.
- [48] H.M. Ledbetter, *Z. Naturforsch.* 31 (1976) 1539.
- [49] F.D. Murnaghan, *Proc. Natl. Acad. Sci. U.S.A.* 30 (1944) 244.
- [50] H. Shiiba, N. Zetsu, M. Nakayama, S. Oishi, K. Teshima, *J. Phys. Chem. C* 119 (2015) 9117.
- [51] J.J. Melo Quintero, K.L. Salcedo Rodríguez, C.E. Rodríguez Torres, L.A. Errico, *J. Alloys Compd.* 775 (2019) 1117.
- [52] X.W. Zhou, H.N.G. Wadley, *J. Phys. Condens. Matter* 17 (2005) 3619.
- [53] F.H. Streitz, J.W. Mintmire, *Phys. Rev. B* 50 (1994), 11996.
- [54] C. Soontrapa, Y. Chen, *Comput. Mater. Sci.* 50 (2011) 3271.
- [55] J.G. Monsalve, C. Ostos, E. Ramos, J.G. Ramírez, O. Arnache, *Curr. Appl. Phys.* 22 (2021) 77.